Journal of Hazardous Materials 186 (2011) 1713–1719

Contents lists available at ScienceDirect

Journal of Hazardous Materials

journal homepage: www.elsevier.com/locate/jhazmat

Arsenate adsorption and desorption kinetics on a Fe(III)-modified montmorillonite

Carina Luengo [a], Virginia Puccia [a], Marcelo Avena [a,b,*]

[a] INQUISUR, Departamento de Química, Universidad Nacional del Sur, Bahía Blanca, Argentina
[b] Consejo de Investigaciones Científicas y Técnicas de Argentina (CONICET), Argentina

ARTICLE INFO

Article history:
Received 12 October 2010
Accepted 14 December 2010
Available online 25 December 2010

Keywords:
Adsorption
Desorption
Arsenate
Modified montmorillonite
Iron surface coatings

ABSTRACT

The adsorption–desorption kinetics of arsenate on a Fe(III)-modified montmorillonite (Fe-M) was studied at different arsenate concentrations, pH and stirring rates. The synthesized solid was a porous sample with Fe(III) present as a mix of monomeric and polymeric Fe(III) species in the interlayer and on the external surface. Adsorption took place in a two-step mechanism, with an initial fast binding of arsenate to Fe(III) species at the external surface (half-lives of 1 min or shorter) followed by a slower binding to less accessible Fe(III) species in pores and the interlayer (half-lives of around 1 h). Desorption kinetics also reflected the presence of externally and internally adsorbed arsenate. At pH 6 the maximum adsorbed arsenate was 52 μmol/g, a value that is low as compared to adsorption on ferrihydrite (700 μmol/g) and goethite (192–220 μmol/g). However, since the Fe(III) content of Fe-M is much lower than that of ferrihydrite and goethite, Fe(III) species in Fe-M are more efficient in binding arsenate than in ferrihydrite or goethite (one As atom is attached every 8.95 iron atoms). This high binding efficiency indicates that Fe(III) species are well spread on montmorillonite, forming small oligomeric species or surface clusters containing just a few iron atoms.

1. Introduction

The presence of arsenic (As) in drinking water is the most common cause of chronic arsenic poisoning in people. This is an important problem especially in countries or locations where people depend on groundwater for drinking [1,2].

The As concentration in groundwater is usually controlled by natural geochemical processes, where adsorption–desorption reactions of As species on mineral surfaces play a key role. These adsorption–desorption processes usually control the speciation of As and thus affect its mobility, toxicity, and bioavailability [2]. Adsorption–desorption processes are also important to develop water purification technologies, with the aim of removing As from water [1,3–6].

Arsenate adsorption has been studied using a variety of adsorbents. Most of the studies were performed using Fe(III) (hydr)oxides, which show high adsorption capacities [7–13]. The adsorption of arsenate, for example, is around 700 μmol/g on ferrihydrite [14], and around 200 μmol/g on goethite [14,15]. There is also considerable information on arsenate adsorption on phyllosilicates, which are among the most significant geosorbents for ions in subsurface geochemical settings because of the high surface area of most phyllosilicates. However, arsenate adsorption on these materials is much lower than on iron containing minerals. For example, Frost and Griffin [16] observed that arsenate sorption onto kaolinite and montmorillonite exhibited a maximum at about pH 5.0 and was around 6.3 μmol/g and 8.4 μmol/g, respectively. Manning and Goldberg [17] reported arsenate adsorption maxima at pH 5.0–6.5 ranging from 0.15 to 0.22 μmol/g on kaolinite, montmorillonite and illite. Li et al. [18] observed an arsenate adsorption maximum on kaolinite of around 2 μmol/g, whereas Saada et al. [19] observed adsorption values of around 1 μmol/g, also on kaolinite. Even though phyllosilicates have a high surface area, most of it corresponds to basal surfaces, which do not adsorb anions significantly because of the presence of negative structural charges. Arsenate adsorption on phyllosilicates takes place mainly at exposed crystal edges. Since edges represent only a small fraction of the total clay surface area, adsorption is relatively low.

The surface properties of phyllosilicates can be greatly modified by the presence of Fe(III) species in the interlayer or by Fe(III) (hydr)oxide surface coatings [20]. Fe(III)-modified phyllosilicates can be found in natural soils and sediments and can be also prepared in the laboratory [21–23]. Such modifications may induce a severe change in both surface and pore structures and thus may change clay adsorption and desorption properties [24]. In a previous work [21], for example, it was shown that modification of

* Corresponding author at: INQUISUR, Departamento de Química, Universidad Nacional del Sur, Av. Alem 1253, 8000 Bahía Blanca, Argentina.
Tel.: +54 291 4595101x3593; fax: +54 291 4595160.
E-mail address: mavena@uns.edu.ar (M. Avena).

0304-3894/$ – see front matter © 2010 Elsevier B.V. All rights reserved.
doi:10.1016/j.jhazmat.2010.12.074

a montmorillonite with Fe(III) species significantly increased the phosphate adsorption capacity of the solid. Ramesh et al. [1], on the other hand, reported an important arsenate adsorption on an Al/Fe-modified montmorillonite.

The aim of this article is to study the adsorption–desorption of arsenate on a Fe(III)-modified montmorillonite. After a general characterization of the synthesized solid, adsorption–desorption kinetics data are presented and analyzed. The effects of pH on adsorption kinetics and the effects of residence times on desorption kinetics are mainly investigated in order to get insight into the processes and mechanisms that control arsenate binding to Fe(III)-modified phyllosilicates.

2. Materials and methods

2.1. Synthesis of the Fe(III)-modified montmorillonite (Fe-M)

The Fe-M sample was prepared from a sodium-exchanged montmorillonite (Na-M), which was obtained from a bentonite deposit in the province of Rio Negro, North Patagonia, Argentina. The sample is identical to sample 11 in a previous study by Lombardi et al. [25], who performed a general chemical characterization of the solid. It is predominantly a sodium-exchanged montmorillonite (99% purity) with minor impurities of quartz, zeolite, feldspar, and calcite. Its CEC is 1.05 mEq/g and its total iron content is 38 mg/g.

Fe-M was prepared by adding 2 L of a 0.035 M $Fe(NO_3)_3$ solution (pH 2.2) to 100 g of Na-M. The resulting dispersion was shaken during 2 h followed by sedimentation and supernatant withdrawal. A new 0.035 M $Fe(NO_3)_3$ solution was added, and the procedure involving shaking, sedimentation and supernatant withdrawal was repeated. The solid was then washed with distilled water until the conductivity was lower than 10 $\mu S\,cm^{-1}$. The final pH of the washed dispersion was around 4.2. Finally, the solid was freeze-dried until a dry powder was obtained.

2.2. Characterization of Fe-M

All characterization techniques were applied to Fe-M. In some cases, and for comparison, the techniques were also used to characterize the Na-M sample.

The iron content was determined by extraction with HCl following the method reported by Ulery and Drees [26]. 50 mg of solid were treated with 10 mL of concentrated HCl (12 M) at 60–80 °C for 1 h. The dispersion was then centrifuged and the supernatant separated for iron analysis using the colorimetric tiocianate method [27] reading the absorbance at 475 nm.

Powder X-ray diffraction patterns were measured with a Rigaku Geigerflex diffractometer between 2° and 40° 2θ using Cu Kα radiation. The specific surface area was measured by BET N_2-adsorption/desorption 77 K with a Quantachrome Nova 1200e instrument wherein the samples were degassed under vacuum during 1 h at 30 °C. Thermo-gravimetric (TG) and differential thermal analysis (DTA) were carried out with a Rigaku Thermoflex TG 8110 equipment with a heating rate of 10 °C/min in air.

2.3. Batch adsorption and desorption kinetics

The adsorption and desorption kinetics experiments were carried out in a cylindrical, water-jacketed reaction vessel covered with a glass cap. Mixing was done by a magnetic stirrer, and carbon dioxide contamination was avoided by bubbling water-saturated N_2. The reaction temperature was maintained at 25 ± 0.2 °C by circulating water through the jacket with a FAC (Argentina) water bath/circulator.

Before starting an adsorption–desorption kinetics experiment, a stock Fe-M suspension (81.6 g/L) was prepared by adding solid Fe-M to a 0.1 M KNO_3 solution. The pH of the resulting suspension was then adjusted to 6.0 (or other desired value) by adding HNO_3 or KOH solutions.

In the adsorption kinetics experiment, 100 mL of a 0.1 M KNO_3 solution containing a known concentration of arsenate were placed in the reaction vessel, and the stirring (450 rpm, except for the cases where effects of stirring rate were investigated), N_2 bubbling and water circulation were switched on. Once the temperature reached the desired value, the pH of the KNO_3–arsenate solution was adjusted to the same pH value of the stock Fe-M suspension. The kinetic experiment was started by adding 320 μL of the stock suspension to the KNO_3–arsenate solution in the reaction vessel. This time was set as the initial time of the adsorption reaction. At different adsorption times, a 5 mL aliquot was withdrawn, centrifuged at 5000 rpm during 5 min and the supernatant extracted for arsenate analysis. The reaction was followed for 360 min and the pH was continuously checked and kept constant by adding minute volumes of concentrated KOH or HNO_3 solutions.

In the desorption kinetics experiment, the arsenate adsorption was carried out as commented above at 25 °C, pH 6.0, 450 rpm and 5.47×10^{-5} M initial arsenate concentration. The adsorption was followed during different times (10 min, 1 h, 18 h and 72 h), which are called from now on residence times. When the residence times finished, the pH of the dispersion was increased to 9.5 adding a concentrated KOH solution by adding a concentrated KOH solution. This time was set as the initial time of the desorption reaction. At different desorption times, a 5 mL aliquot was withdrawn, centrifuged at 5000 rpm during 5 min and the supernatant extracted for arsenate analysis. The reaction was followed during 360 min and the pH was continuously checked and kept constant by adding small volumes of concentrated KOH or HNO_3 solutions.

Arsenate concentrations were measured by the spectrophotometric method proposed by Murphy and Riley [28]. Adsorbed arsenate was calculated from the difference between the initial arsenate concentration and the concentration that remained in the supernatant solution.

In all experiments the pH was measured with a Crison GLP 22 pH meter and a Radiometer GH2401 combined pH electrode. The stirring of the dispersions was controlled with an IKA RH KT/C magnetic stirrer. Spectrophotometric determinations were performed using an Agilent 8453 UV–vis diode array spectrophotometer equipped with a 1-cm quartz cell. All the solutions were prepared from analytical reagent grade chemicals.

3. Results and discussion

3.1. Characterization of Fe-M

The distribution of Fe(III) species in the 0.035 M $Fe(NO_3)_3$ solution used to prepare Fe-M was calculated using the software MINEQL+ 3.01b [29] with equilibrium constants already included in the software. These constants can be also found in a previous publication [21]. At pH 2.2 the solution was unsaturated with respect to ferrihydrite and all Fe(III) species were in the dissolved state. The main species present in the solution were Fe^{3+} (0.0120 M), $Fe(OH)^{2+}$ (0.0124 M), $Fe_2(OH)_2{}^{4+}$ (0.0041 M) and $Fe_3(OH)_4{}^{5+}$ (5.7×10^{-4} M), which represent, respectively, 34%, 35%, 23% and 5% of the total Fe(III) concentration in the solution. All of them are positively charged species with high affinity for the montmorillonite surface. In fact, an uncoloured supernatant was obtained after the first treatment of Na-M with the 0.035 M $Fe(NO_3)_3$ solution, revealing that most of the Fe(III) species were removed from solution by the solid.

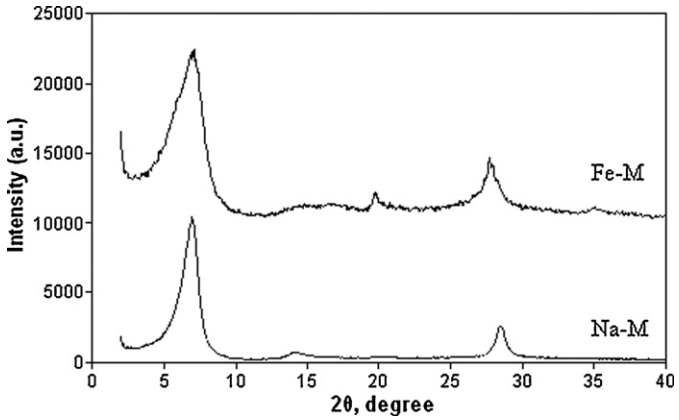

Fig. 1. DRX of Na-M and Fe-M. The scale for Fe-M was multiplied by a factor of 4.5 and added a factor of 9000 to better visualize the diffractogram.

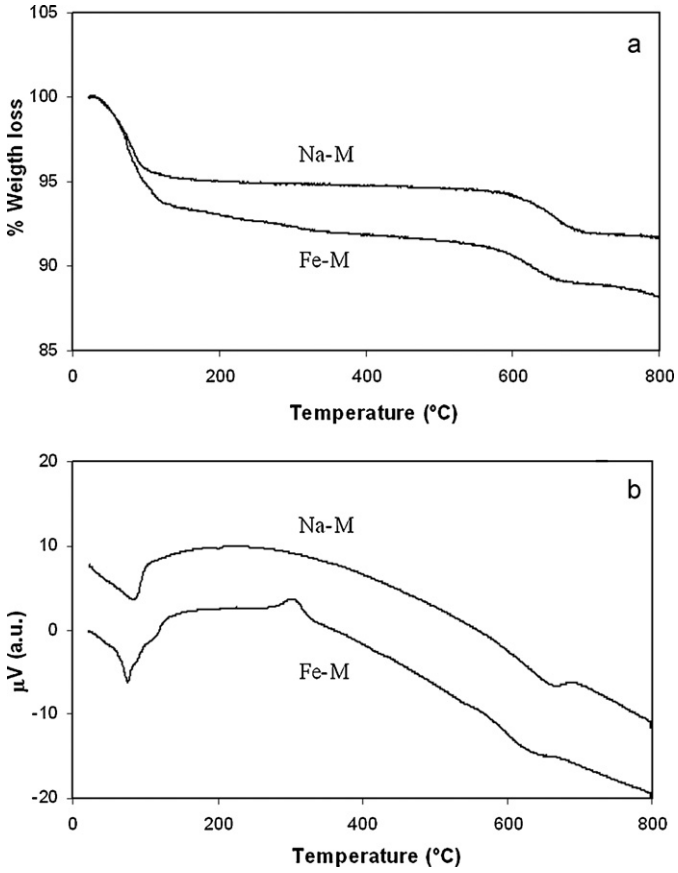

Fig. 2. TG/DTA curves of Na-M and Fe-M. (a) TG and (b) DTA.

The iron content of the studied solids as measured by the HCl extraction method was 4 mg/g for Na-M and 26 mg/g for Fe-M. The method cannot extract structural iron from Na-M since only 4 mg/g out of the total 38 mg/g were extracted. The 4 mg/g value may represent the content of minor non-structural iron impurities. If this amount of iron is assumed to be present also in Fe-M, the net amount of iron that was incorporated during the synthesis of Fe-M was 22 mg/g.

The powder X-ray diffractograms of Na-M and Fe-M are shown in Fig. 1. The 0 0 1 reflection of Na-M was rather intense and appeared at 6.95° 2θ (d_{001} = 12.7 Å), value that is normal for sodium-exchanged montmorillonites [30–32]. A less intense and broader 0 0 1 reflection was observed for Fe-M, with a maximum at 7.05° 2θ (d_{001} = 12.5 Å) and a shoulder at around 6.2° 2θ (d_{001} = 14.3 Å). The decrease in intensity and the broadening of the reflection indicate that the staking of layers in Fe-M is more disordered than in the case of Na-M. Literature reports regarding the effects of Fe(III) species on the basal spacing of montmorillonite are varied. Borgnino et al. [21] found a small decrease in the basal spacing after modification with Fe(III) and attributed it to the smaller radii of Fe^{3+} and $[Fe(OH_2)_6]^{3+}$ ions as compared to those of Na^+ and $[Na(OH_2)_6]^+$ ions. Decrease in d_{001} by addition of Fe(III) has been also observed by Chen et al. [30], who attributed this effect to strong attractive forces between interlayer iron and the silicate sheets of montmorillonite. Other authors, on the contrary, have observed a slight increase in d_{001} due to the presence of polymeric species of Fe(III) within the interlayer [33,34]. Data in Fig. 1 suggest both cases of intercalation, with monomeric and polymeric Fe(III) species, resulting in a more disordered staking. Most of the reports where Fe(III)-modified montmorillonites were studied also indicate or assume the presence of Fe(III) (hydr)oxide phases coating the surface [21,31]. No strong evidences for the formation of a separate Fe(III) (hydr)oxide phase were found with XRD. Perhaps, the weak reflection at around 35° 2θ shown by Fe-M is due to the presence of some ferrihydrite coatings.

The surface areas measured by BET N_2 were 1.4 and 20.7 m^2/g for Na-M and Fe-M, respectively. They represent the external areas of the solids, since nitrogen molecules cannot enter the interlayer space. The increase in the area by incorporating Fe(III) is also an evidence for the more disordered staking of layers in Fe-M. In addition, it may also indicate the presence of Fe(III) (hydr)oxides phases coating the surface of montmorillonite. Ferrihydrite, for example, has a surface area of 300 m^2/g [35] or even 600 m^2/g [36,37] and small amounts of this solid would significantly contribute to increase the BET surface area. Based on N_2-adsorption/desorption isotherms, an average pore volume of 0.05 cm^3/g and an average pore radius of 20.1 Å were obtained for Fe-M. These results are very similar to those reported by Manjanna et al. [38] and Nguyen-Thanh et al. [39], who showed that modification with Fe(III) generated small pores in the solid and increased the BET area.

TG/DTA curves of Na-M and Fe-M are shown in Fig. 2. There were two main weight losses in the TG curves for both samples, the first one due to the release of water coordinating interlayer cations and water adsorbed on the particle surface (below 120 °C), and the second one due to the dehydroxylation of structural OH groups (between 500 and 700 °C). The DTA curve of Na-M showed two endothermic peaks at 83 °C and 664 °C corresponding to the two water releases commented above for the TG curve. These peaks were also observed by Lenoble et al. [40], Vargas Rodríguez et al. [41] and Vieira Coelho et al. [42]. The DTA curve of Fe-M was more complex showing two endothermic processes at 74 °C and 115 °C due to dehydration, one endothermic process at 604 °C due to dehydroxylation, and an exothermic process at 302 °C. The dehydration process in Fe-M is different to that of Na-M due to the presence of Fe(III) species in the interlayer and on the external surface, since the hydration energy of Na(I) and Fe(III) are different. The exothermic peak at 302 °C indicates a structural change in Fe-M. This peak must be due to a structural change on an iron (hydr)oxide phase coating the clay surface. Ferrihydrite, for example, shows exothermic peaks at around 291 °C [43,44].

In summary, the characterization of the synthesized sample by XRD, surface area and porosity measurement and TG/DTA indicates that iron is present as a mix of monomeric and polymeric Fe(III) species in the interlayer and on the external surface. There may exist also some surface coatings with Fe(III) (hydr)oxides such as ferrihydrite.

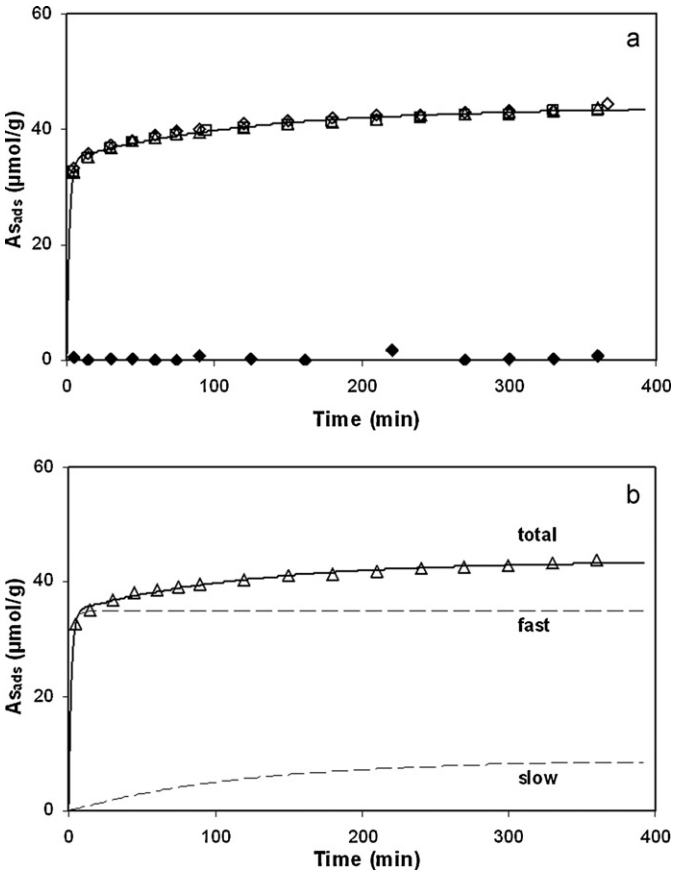

Fig. 3. (a) Adsorption kinetics of arsenate on Na-M (♦) (at 450 rpm) and Fe-M (at different stirring rates: (◊) 250 rpm; (△) 450 rpm; (□) 650 rpm) at 25 °C and pH 6.0. Initial concentration of arsenate: 5.57×10^{-5} M. Line in the figure corresponding to 450 rpm was calculated with Eq. (1) and parameter listed in Table 1. (b) Adsorption kinetics of arsenate on Fe-M (△) at 450 rpm. Initial concentration of arsenate: 5.57×10^{-5} M. Line was calculated with Eq. (1) and parameter listed in Table 1.

3.2. Arsenate adsorption

Fig. 3a shows the arsenate adsorption kinetics on Na-M and Fe-M at pH 6 and 25 °C at the same initial arsenate concentration (5.57×10^{-5} M). Arsenate adsorption on Fe-M was relatively fast during the first 5 min of reaction (first measured point), where adsorption was 29 µmol/g. A slower adsorption took place after 5 min, increasing up to around 41 µmol/g at 360 min of reaction. This value was rather high as compared to the adsorption on Na-M under the same conditions (around 0.8 µmol/g). The low adsorption on Na-M is well known for anionic adsorbates and is mainly due to the presence of unreactive siloxane groups at the Na-M basal surface and to the presence of negative structural charges within the clay structure. Since adsorption on Na-M is negligible as compared to adsorption on Fe-M, it is clear that adsorption on Fe-M is due to the presence of Fe(III) species, which create favourable adsorption sites for arsenate species.

Fig. 3a also shows arsenate adsorption on Fe-M at different stirring rates. All curves were equal, indicating that adsorption was not controlled by diffusion processes on the aqueous side of the solid/water interface.

Adsorption vs. t curves as shown in Fig. 3a for arsenate on Fe-M, with most of the adsorption taking place quickly during the first 5 min of reaction and the rest of adsorption taking place at a slower rate, were found at all investigated conditions (see below). The shape of these curves is typical for the adsorption of oxoanions such as phosphate and arsenate on iron (hydr)oxides [9]. For adsorption on goethite, for example, it was proposed that the fast adsorption during the first reaction minutes was due to the binding of oxoanions to the outer surface of goethite, and the rest of the adsorption was slower because of pore diffusion or intraparticle diffusion [9]. Fast adsorption on external sites combined with a slower diffusion into pores was also proposed for arsenate adsorption on ferrihydrite by Fuller et al. [45]. A similar mechanism can be proposed for arsenate adsorption on Fe-M, with an initial fast binding of arsenate to Fe(III) species at the external surface (adsorbed species and surface coatings) followed by a slower binding to less accessible Fe(III) species in pores and perhaps the interlayer. It must be remarked that this mechanism is very simplified for the case of Fe-M. A detailed description of arsenate adsorption kinetics on Fe-M is difficult owing to the difficulty of the material structure and chemistry. The separate behaviour of the different Fe(III) species (species in the interlayer, at the external surface, surface coatings) should be considered along with the presence of pores in the solid. In spite of it, this simplified mechanism captures the basics of arsenate adsorption on Fe-M, indicating that adsorption occurs in two different processes, with two different time scales.

The adsorption kinetics with two different time scales can be represented in a simple way by the following equation:

$$A = A_1(1 - e^{-k_1 t}) + A_2(1 - e^{-k_2 t}) \quad (1)$$

where A is the total adsorbed amount of arsenic at time t and the terms $A_1(1 - e^{-k_1 t})$ and $A_2(1 - e^{-k_2 t})$ are first-order kinetic terms representing the adsorbed amounts in the fast and slow processes, respectively. A_1 and A_2 are the respective adsorbed amounts after equilibration is reached, and k_1 and k_2 are the respective rate constants for the fast and slow processes. The fit of kinetic data with Eq. (1) does not allow the determination of a reaction mechanism due to the complexity of the studied system [45], and it is only used here for a better identification of the fast and slow adsorption processes. The predictions of Eq. (1), using the parameters listed in Table 1, are plotted in Fig. 3a and compared to experimental data. The same data, although only those obtained at a stirring rate of 450 rpm, are also shown in Fig. 3b together with the calculated

Table 1
Optimized parameters for arsenate adsorption on Fe-M.

T (°C)	pH	Concentration (M, 10^{-5})	Stirring rate (rpm)	A_1 (µmol/g)	K_1 (min^{-1})	A_2 (µmol/g)	K_2 (min^{-1})	R^2
25	6.0	2.81	450	24.20	0.65	2.23	0.0139	0.9951
25	6.0	3.50	450	30.30	0.60	3.55	0.0251	0.9484
25	6.0	4.18	450	33.06	0.56	5.57	0.0102	0.9929
25	6.0	5.57	450	34.78	0.53	8.94	0.0082	0.9919
25	6.0	6.85	450	37.85	0.52	11.25	0.0076	0.9948
25	6.0	8.15	450	40.37	0.54	12.30	0.0067	0.9900
25	4.5	5.57	450	37.92	0.47	11.73	0.0109	0.9955
25	7.5	5.57	450	24.69	0.55	8.28	0.0067	0.9744
25	9.0	5.57	450	14.99	0.59	6.27	0.0063	0.9433
25	6.0	5.57	250	35.14	0.56	8.85	0.0087	0.9914
25	6.0	5.57	650	34.59	0.53	8.65	0.0088	0.9918

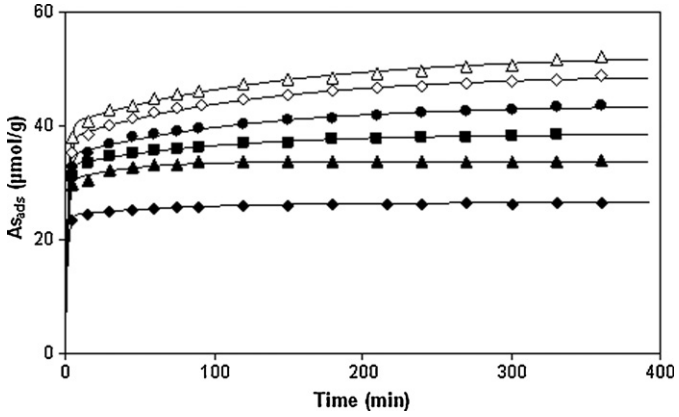

Fig. 4. Adsorption kinetics of arsenate on Fe-M at different initial concentrations of arsenate: (♦) 2.81×10^{-5} M, (▲) 3.50×10^{-5} M, (■) 4.18×10^{-5} M, (●) 5.57×10^{-5} M, (◊) 6.85×10^{-5} M, (△) 8.15×10^{-5} M. Stirring rate: 450 rpm, pH: 6.0 and temperature: 25 °C. Lines were calculated with Eq. (1) and parameters listed in Table 1.

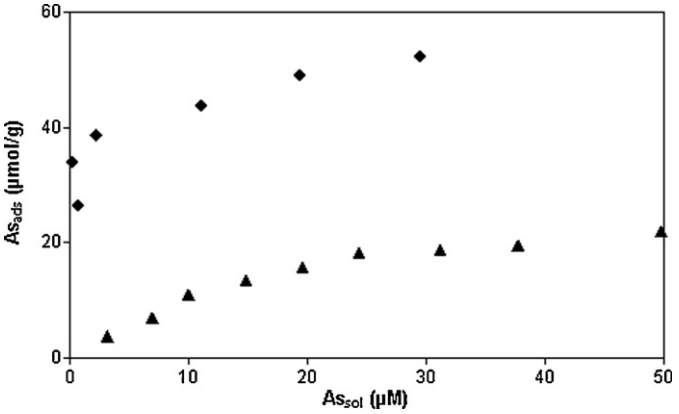

Fig. 6. Adsorption isoterms of arsenate on Fe-M at (♦) pH 6 and (▲) pH 9.5.

adsorptions during the fast and slow processes. Predictions indicate that an adsorption of 29 µmol/g (given by the value of A_1 and corresponding to 70.7% of the adsorption) takes place quickly and that the remaining adsorption of 12 µmol/g (given by the value of A_2 and corresponding to 29.3% of the adsorption) takes place more slowly. The differences in the values of k_1 and k_2 reflect the different time scales of the two adsorption processes (half-lives in the order of 1 min and in the order of 1 h, respectively). Actually, the value of k_1 only represents a lower limit for this rate constant. Data points at times much shorter than 5 min would be necessary to accurately evaluate its value.

The effects of initial arsenate concentration on the adsorption kinetics are shown in Fig. 4, and the effects of pH are shown in Fig. 5. At a given time, arsenate adsorption increased by increasing the oxoanion concentration and decreased by increasing pH. This pH dependency is well known for adsorption of oxoanions on Fe(III) containing minerals such as ferrihydrite and goethite [36,46,47]. Lines in the figures were also calculated with Eq. (1) using parameters listed in Table 1, showing that the two-step kinetics operates under all investigated conditions. In all cases the adsorption during the fast process was between 70 and 92% of the total adsorption, the rest took place during the slow process. k_1 was always larger than k_2 with half-lives in the order of 1 min (or lower) for the fast process and around 1 h for the slow process. The results indicate that most of adsorption sites were located on the external surface of Fe-M and were easily and quickly accessed by arsenate.

The experiments at different arsenate concentration allowed to construct an adsorption isotherm at pH 6 by plotting the long-term (360 min) adsorption data as a function of the equilibrium arsenate concentration. This isotherm at pH 6 is shown in Fig. 6 and compared to another isotherm obtained at pH 9.5. The decrease in adsorption by increasing pH indicates that desorption should take place by first adsorbing arsenate at pH 6 and then increasing the pH of the suspension to 9.5. Desorption data at pH 9.5 after adsorbing arsenate at pH 6.5 during different residence times are shown in Fig. 7. Arsenate desorbed in all cases as expected. Desorption should not be complete in these cases because arsenate is always present in the system and thus the reaction should stop when the new equilibrium situation, which is dictated by the isotherm at pH 9.5, is attained. The dashed line in Fig. 7 indicates this new equilibrium situation. Equilibrium was attained rather quickly for short residence times (10 and 60 min). For long residence times the system did not reach equilibrium during the investigated period. This behaviour is consistent with the two-step adsorption mechanism proposed above. Short residence times mean that adsorption took place mainly at the external surface, leading to adsorbed species that were able to pass quickly to solution when the pH was raised to 9.5. Long residence times, on the contrary, mean that a significant part of the adsorbed arsenate was attached to Fe(III) species in pores or the interlayer, resulting in a slower desorption. Unfortunately, there are no articles in the literature about arsenate desorption

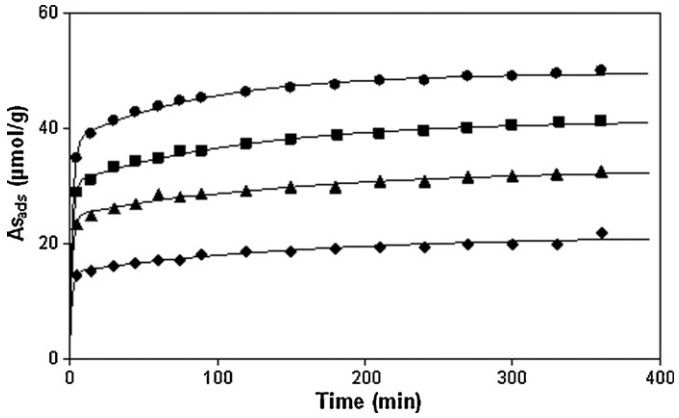

Fig. 5. Adsorption kinetics of arsenate on Fe-M at different pH: (●) 4.5; (■) 6.0; (▲) 7.5; (♦) 9.0. Initial arsenate concentration: 5.57×10^{-5} M. Stirring rate: 450 rpm and temperature: 25 °C. Lines were calculated with Eq. (1) and parameters listed in Table 1.

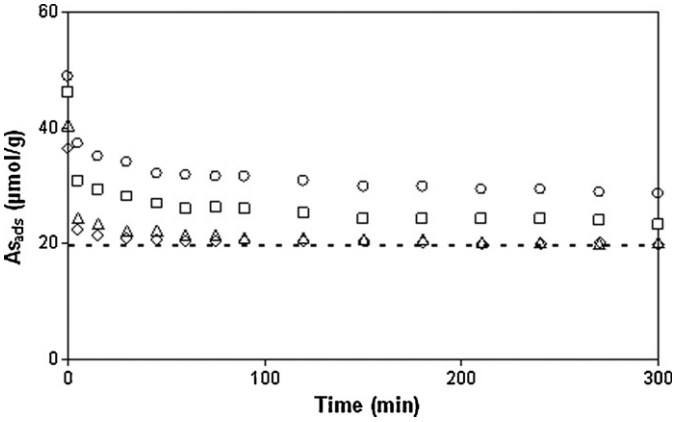

Fig. 7. Desorption kinetics of arsenate on Fe-M at different residence time: (◊) 10 min; (△) 1 h; (□) 18 h; (○) 72 h. Initial arsenate concentration: 5.57×10^{-5} M, adsorption pH: 6.0, desorption pH: 9.5, temperature: 25 °C and stirring rate: 450 rpm. The dashed line represents the equilibrium situation at pH 9.5.

Table 2
Arsenate adsorption capacity of some Fe(III)-containing solids at pH 6.

Adsorbent	Arsenate adsorption at pH 6 (μmol/g)	Fe content (g/g)	Fe/As (mol/mol)	References
Ferrihydrite	700	0.58	14.84	[14]
Goethite	220	0.63	51.27	[14]
Goethite	192	0.63	58.75	[15]
Fe-M	52	0.026	8.95	This work

Goethite formula (FeOOH), ferrihydrite formula ($5Fe_2O_3 \cdot 9H_2O$).

kinetics from Fe(III)-modified montmorillonites. In spite of this, the behaviour is comparable to that of other systems where anions were desorbed from Fe(III) (hydr)oxides. Strauss et al. [48], for example, showed that phosphate adsorbed on goethites of different crystallinity on external and internal (pores) sites. Phosphate that was adsorbed on external sites desorbed faster than that adsorbed on internal sites.

Table 2 compares the arsenate adsorption capacity of several Fe(III) containing minerals reported in the literature. Data corresponds to the maximum adsorption capacity obtained from adsorption isotherms at pH 6. Comparisons of this type with different sorbents are usually done with the aim of choosing the best material to be used to remove arsenic from water and wastewaters [1]. In this sense, it is clear that the studied Fe-M sample is not the best adsorbent. Ferrihydrite, which is formed by very small particles with a large surface area, is the solid that better adsorbs arsenate. In spite of this, data in Table 2 reveal that Fe(III) species in Fe-M are very active in binding arsenate. The ratios Fe/As in the solids show that 1 As atom is attached every 14.84 atoms of iron in ferrihydrite, every 51–59 atoms of iron in goethite and every 8.95 atoms of iron in Fe-M. This high binding efficiency of iron in Fe-M indicates that Fe(III) species are well spread over the montmorillonite surface. They should be mainly present as small oligomeric species or small clusters containing just a few iron atoms.

4. Conclusions

The modification of the Na-M sample with Fe(III) species resulted in an Fe(III)-modified montmorillonite having a mix of monomeric and polymeric Fe(III) species in the interlayer and on the external surface. These Fe(III) species were responsible for arsenate adsorption. Arsenate adsorption took place with an initial fast binding of arsenate to Fe(III) species at the external surface (adsorbed species and perhaps surface coatings) followed by a slower binding to less accessible Fe(III) species in pores and the interlayer. Desorption results also reflected the presence of externally and internally adsorbed arsenate. Even though the synthesized Fe-M sample adsorbs less arsenate than ferrihydrite and goethite, Fe(III) species in Fe-M are more efficient in binding arsenate than in ferrihydrite or goethite. This indicates that Fe(III) species are well spread over the montmorillonite surface.

Acknowledgments

We thank the research group of M.E. Parolo (Universidad del Comahue, Neuquén) for providing the Na-montmorillonite sample. This work was financed by CONICET, CIC, SECyT-Argentina and SECyT-UNS. CL and VP thank CONICET and CIC, respectively, for the doctoral fellowships.

References

[1] A. Ramesh, H. Hasegawa, T. Maki, K. Ueda, Adsorption of inorganic and organic arsenic from aqueous solutions by polymeric Al/Fe modified montmorillonite, Sep. Purif. Technol. 56 (2007) 90–100.
[2] P.L. Smedley, D.G. Kinniburgh, A review of the source, behaviour and distribution of arsenic in natural waters, Appl. Geochem. 17 (2002) 517–568.
[3] K. Gupta, U.C. Ghosh, Arsenic removal using hydrous nanostructure iron(III)–titanium(IV) binary mixed oxide from aqueous solution, J. Hazard. Mater. 161 (2009) 884–892.
[4] B.R. Manna, U.C. Ghosh, Pilot-scale performance of arsenic and iron removal from contaminated groundwater, Water Qual. Res. J. Can. 40 (2005) 82–90.
[5] D. Mohan, C.U. Pittman Jr., Arsenic removal from water/wastewater using adsorbents—a critical review, J. Hazard. Mater. 147 (2007) 1–53.
[6] S. Wang, C.N. Mulligan, Natural attenuation processes for remediation of arsenic contaminated soils and groundwater, J. Hazard. Mater. 138 (2006) 459–470.
[7] M.A. Anderson, J.F. Ferguson, J. Gavis, Arsenate adsorption on amorphous aluminum hydroxide, J. Colloid Interface Sci. 54 (1976) 391–399.
[8] M. Grafe, M.J. Eick, P.R. Grossl, Adsorption of arsenate(V) and arsenite(III) on goethite in the presence and absence of dissolved organic carbon, Soil Sci. Soc. Am. J. 65 (2001) 1680–1687.
[9] C. Luengo, M. Brigante, M. Avena, Adsorption kinetics of phosphate and arsenate on goethite. A comparative study, J. Colloid Interface Sci. 311 (2007) 354–360.
[10] Y. Mamindy-Pajany, C. Hurel, N. Marmier, M. Roméo, Arsenic adsorption onto hematite and goethite, CR Chim. 12 (2009) 876–881.
[11] K.P. Raven, A. Jain, R.H. Loeppert, Arsenite and arsenate adsorption on ferrihydrite: kinetics, equilibrium, and adsorption envelopes, Environ. Sci. Technol. 32 (1998) 344–349.
[12] J.S. Zhang, R. Stanforth, S.O. Pehkonen, Irreversible adsorption of methyl arsenic, arsenate, and phosphate onto goethite in arsenic and phosphate binary systems, J. Colloid Interface Sci. 317 (2008) 35–43.
[13] J. Giménez, M. Martínez, J. de Pablo, M. Rovira, L. Duro, Arsenic sorption onto natural hematite, magnetite, and goethite, J. Hazard. Mater. 141 (2007) 575–580.
[14] M. Pigna, G.S.R. Krishnamurti, A. Violante, Kinetics of arsenate sorption–desorption from metal oxides: effect of residence time, Soil Sci. Soc. Am. J. 70 (2006) 2017–2027.
[15] S.E. O'Reilly, D.G. Strawn, D.L. Sparks, Residence time effects on arsenate adsorption/desorption mechanisms on goethite, Soil Sci. Soc. Am. J. 65 (2001) 67–77.
[16] R.R. Frost, R.A. Griffin, Effect of pH on adsorption of arsenic and selenium from landfill leachate by clay minerals, Soil Sci. Soc. Am. J. 41 (1977) 53–57.
[17] B.A. Manning, S. Goldberg, Modeling arsenate competitive adsorption on kaolinite, montmorillonite and illite, Clays Clay Miner. 44 (1996) 609–623.
[18] Z. Li, R. Beachner, Z. McManama, H. Hanlie, Sorption of arsenic by surfactant-modified zeolita and kaolinite, Micropor. Mesopor. Mater. 105 (2007) 291–297.
[19] A. Saada, D. Breeze, C. Crouzet, S. Cornu, P. Baranger, Adsorption of arsenic(V) on kaolinite and on kaolinite–humic acid complexes: role of humic acid nitrogen groups, Chemosphere 51 (2003) 757–763.
[20] J. Zhuang, G.R. Yu, Effects of surface coatings on electrochemical properties and contaminant sorption of clay minerals, Chemosphere 49 (2002) 619–628.
[21] L. Borgnino, M.J. Avena, C.P. De Pauli, Synthesis and characterization of Fe(III)-montmorillonites for phosphate adsorption, Colloids Surf. A: Physicochem. Eng. Aspects 341 (2009) 46–52.
[22] K. Hanna, Adsorption of aromatic carboxylate compounds on the surface of synthesized iron oxide-coated sands, Appl. Geochem. 22 (2007) 2045–2053.
[23] W.H. Hendershot, L.M. Lavkulich, Effect of sesquioxide coatings on surface charge of standard mineral and soil samples, Soil Sci. Soc. Am. J. 47 (1983) 1252–1260.
[24] R.S. Juang, S.H. Lin, F.C. Huang, C.H. Cheng, Structural studies of Na-montmorillonite exchanged with Fe^{2+}, Cr^{3+}, and Ti^{4+} by N_2 adsorption and EXAFS, J. Colloid Interface Sci. 274 (2004) 337–340.
[25] B. Lombardi, M. Baschini, R.M. Torres Sánchez, Bentonita deposits of Northern Patagonia, Appl. Clay Sci. 22 (2003) 309–312.
[26] A.L. Ulery, L.R. Drees, Methods of Soil Analysis. Part 5. Mineralogical Methods, Soil Science Society of America, Madison, WI, 2008.
[27] P.H. Hsu, Determination of iron with thiocyanate, Soil Sci. Soc. Am. J. 31 (1967) 353–355.
[28] J. Murphy, J.P. Riley, A modified single solution method for the determination of phosphate in natural waters, Anal. Chim. Acta 27 (1962) 31–36.
[29] J. Westall, J.L. Zachary, F.M.M. Morel, A Computer Program for the Calculation of Chemical Equilibrium Composition of Aqueous Systems, Massachussets Institute of Technology, Cambridge, MA, 1976.
[30] G. Chen, B. Han, H. Han, Interaction of cationic surfactants with iron and sodium montmorillonite suspensions, J. Colloid Interface Sci. 201 (1998) 158–163.
[31] J. Manjanna, Preparation of Fe(II)-montmorillonite by reduction of Fe(III)-montmorillonite with ascorbic acid, Appl. Clay Sci. 42 (2008) 32–38.
[32] P. Yuan, H. He, F. Bergaya, D. Wu, Q. Zhou, J. Zhu, Synthesis and characterization of delaminated iron-pillared clay with meso–microporous structure, Micropor. Mesopor. Mater. 88 (2006) 8–15.

[33] J.P. Chen, M.C. Hausladen, R.T. Yang, Delaminated Fe_2O_3-pillared clay: its preparation, characterization, and activities for selective catalytic reduction of No by NH_3, J. Catal. 151 (1995) 135–146.
[34] H. Dramé, Cation exchange and pillaring of smectites by aqueous Fe nitrate solutions, Clays Clay Miner. 53 (2005) 335–347.
[35] H. Green-Pedersen, N. Pind, Preparation, characterization, and sorption properties for Ni(II) of iron oxyhydroxide–montmorillonite, Colloids Surf. A: Physicochem. Eng. Aspects 168 (2000) 133–145.
[36] J. Antelo, S. Fiol, C. Pérez, S. Mariño, F. Arce, D. Gondar, R. López, Analysis of phosphate adsorption onto ferrihydrite using the CD-MUSIC model, J. Colloid Interface Sci. 347 (2010) 112–119.
[37] T. Hiemstra, J. Antelo, R. Rahnemaie, W.H. van Riemsdijk, Nanoparticles in natural systems I: the effective reactive surface area of the natural oxide fraction in field simples, Geochim. Cosmochim. Acta 74 (2010) 41–58.
[38] J. Manjanna, T. Kozaki, S. Sato, Fe(III)-montmorillonite: basic properties and diffusion of tracers relevant to alteration of bentonite in deep geological disposal, Appl. Clay Sci. 43 (2009) 208–217.
[39] D. Nguyen-Thanh, K. Block, T.J. Bandosz, Adsorption of hydrogen sulfide on montmorillonites modified with iron, Chemosphere 59 (2005) 343–353.
[40] V. Lenoble, O. Bouras, V. Deluchat, B. Serpaud, J.C. Bollinger, Arsenic adsorption onto pillared clays and iron oxides, J. Colloid Interface Sci. 255 (2002) 52–58.
[41] Y.M. Vargas-Rodríguez, V. Gómez-Vidales, E. Vázquez-Labastida, A. García-Bórquez, G. Aguilar-Sahagún, H. Murrieta-Sánchez, M. Salmón, Caracterización espectroscópica, química y morfológica y propiedades superficiales de una montmorillonita mexicana, Rev. Mex. Cienc. Geol. 25 (2008) 135–144.
[42] A.C. Vieira Coelho, G. Poncelet, J. Ladrière, Nickel, iron-containing clay minerals from Niquelândia deposit, Brazil: 1. Characterization, Appl. Clay Sci. 17 (2000) 163–181.
[43] R.M. Cornell, U. Schwertmann, The Iron Oxides. Structure, Properties, Reactions, Occurrence and Uses, VCH Publishers, New York, 1996.
[44] J.L. Jambor, J.E. Dutrizac, Occurrence and constitution of natural and synthetic ferrihydrite, a widespread iron oxyhydroxide, Chem. Rev. 98 (1998) 2549–2585.
[45] C.C. Fuller, J.A. Davis, G.A. Waychunas, Surface chemistry of ferrihydrite: part 2. Kinetics of arsenate adsorption and coprecipitation, Geochim. Cosmochim. Acta 57 (1993) 2271–2282.
[46] J. Antelo, M. Avena, S. Fiol, R. López, F. Arce, Effects of pH and ionic strength on the adsorption of phosphate and arsenate at the goethite–water interface, J. Colloid Interface Sci. 285 (2005) 476–486.
[47] T. Hiemstra, W.H. van Riemsdijk, Surface structural ion adsorption modeling of competitive binding of oxyanions by metal (hydr)oxides, J. Colloid Interface Sci. 210 (1999) 182–193.
[48] R. Strauss, G.W. Brümmer, N.J. Barrow, Effects of crystallinity of goethite: II. Rates of sorption and desorption of phosphate, Eur. J. Soil Sci. 48 (1997) 101–114.